Department of Hospital Pharmacy, Suqian First Hospital, Suqian, People's Republic of China

20(S)-Ginsenoside Rg3 regulates the Hedgehog signaling pathway to inhibit proliferation and epithelial-mesenchymal transition of lung cancer cells

Ning Cai, Qing Yang, Dao-Biao Che*, Xin Jin*

Received April 30, 2021, accepted June 4, 2021

**Corresponding authors: Dao-Biao Che, Xin Jin, Department of Hospital Pharmacy, Suqian First Hospital,120 Suzhi road, Suqian 223800, People's Republic of China*
chedaobiao@126.com, jinxin871211@163.com

Pharmazie 76: 431-436 (2021) *doi: 10.1691/ph.2021.1573*

20(*S*)-Ginsenoside Rg3 (S-Rg3) has good antitumor activity and has been used in clinical oral antitumor therapy. However, the effect of S-Rg3 on the Hedgehog (Hh) signaling pathway has not been reported. In this study, we used CCK8, cell wound healing, Transwell, and western blotting assays as well as small interfering RNA to decrease GLI1 protein expression to investigate the effect of S-Rg3 on the Hh pathway in A549 cells. The results showed that S-Rg3 substantially inhibited the proliferation, migration, and invasion of A549 cells in a concentration-dependent manner. Furthermore, S-Rg3 had significant regulatory effects on PTCH1 and GLI1, key proteins in the Hh pathway, causing significant upregulation of PTCH1 levels and downregulation of GLI1 expression. After silencing the Hh signaling pathway, the inhibitory effect of S-Rg3 administration on the expression of epithelial mesenchymal transition-related proteins was further enhanced. Molecular dynamics simulations showed that Rg3 molecules could bind stably to PTCH1 protein through hydrophobic interactions, hydrogen bonds, and π-π stacking forces. Thus, S-Rg3 can regulate Hh signaling pathway transduction in A549 cells to inhibit lung cancer cell proliferation, migration, invasion, and epithelial mesenchymal transition.

1. Introduction

Lung cancer poses a serious threat to human health and life. According to Global Cancer Statistics 2020 (Ferlay et al. 2021), the incidence rate of lung cancer (11.4%) is second only to that of breast cancer (11.8%). Furthermore, among cancers, lung cancer is associated with the highest mortality rate worldwide. Thus, the burden of lung cancer continues to grow. Metastasis and recurrence present difficulties to lung cancer treatment and are the root cause of treatment failure. Brain, bone, and liver metastases are the three major modes of metastasis in advanced non-small cell lung cancer (NSCLC). Chemotherapy, radiotherapy, targeted therapy, and immunotherapy, which are the most commonly used treatments for metastasis, significantly affect the prognosis of patients.

The initiation phase of metastasis, which comprises cell migration and invasion, is activated by epithelial-mesenchymal transition (EMT) (Thiery et al. 2009; Cao et al. 2016). EMT is the transformation and differentiation of polar epithelial cells to mesenchymal cells under specific conditions (Li et al. 2021) and plays a key role in tumor formation and pathogenesis. It has been shown that multiple signaling pathways are involved in the regulation of tumor EMT (Gao et al. 2015).

The Hedgehog (Hh) signaling pathway is an essential regulatory mechanism in embryonic development and tissue and organ formation (Wang et al. 2013; Belgacem and Borodinsky 2015). The Hh pathway involves three homologous ligands, Sonic hedgehog, Indian hedgehog, and Desert hedgehog, which bind to the receptors Patched (PTCH) and release Smoothened. This leads to the activation of glioma-associated oncogene-1 (GLI1), which activates transcription (Pan and Zhou 2012). Clinical studies (Dai et al. 2011; Bailey et al. 2009) have shown that metastasis and prognosis are closely related to the Hh signaling pathway. Additionally, it has been reported (Chen et al. 2011; Li et al. 2018) that EMT transcription factors are target genes for Hh signal transduction in poorly differentiated liver cancer cells. The activation of the Hh signaling pathway can lead to cell proliferation, EMT, and cell survival (Scales and de Sauvage 2009).

The main active ingredient of the widely used clinical traditional Chinese medicine (TCM) preparation, Shenyi capsule, is ginsenoside Rg3, which has multiple pharmacological activities, including antiinflammatory, antitumor, neuroprotective, and antidepressant effects (Hien et al. 2010). However, it has two epimers, among which the 20(S)-ginsenoside Rg3 isomer (S-Rg3) promotes the senescence and apoptosis of gallbladder tumor cells via the P53 signaling pathway (Zhang et al. 2015). S-Rg3 can also inhibit EMT in ovarian cancer (Li et al. 2017). However, the effect of S-Rg3 on the Hh pathway has not been investigated. Therefore, the aim of the present study was to determine whether S-Rg3 affects the Hh signaling pathway and lung cancer cell metastasis using cell proliferation, migration, and invasion assays, as well as western blotting and qPCR.

2. Investigations and results

2.1. S-Rg3 inhibits the proliferation of A549 cells

The cell counting kit-8 (CCK8) assay (Fig. 1A) showed that S-Rg3 inhibited the proliferation of A549 cells after 48 and 72 h of treatment with different concentrations of S-Rg3, and a higher concentration of S-Rg3 produced a stronger inhibitory effect. The IC_{50} values of S-Rg3 at 48 and 72 h were 253.101 and 73.618 μg/mL, respectively. The results of the cell clone formation assay are shown in Fig. 1B. Treatment with 25, 75, and 125 μg/mL S-Rg3 for 72 h had significant, concentration-dependent, inhibitory effects on clone formation, as a significant decrease in the colony formation rate was observed as the concentration of S-Rg3 increased. The EdU live-cell assay (Fig. 1C) showed that the positive rate of live cells significantly decreased with the increase in S-Rg3 concentration, which suggests that the proliferation ability of cells was significantly inhibited. The positive rate of live cells was lower in the 125 μg/mL

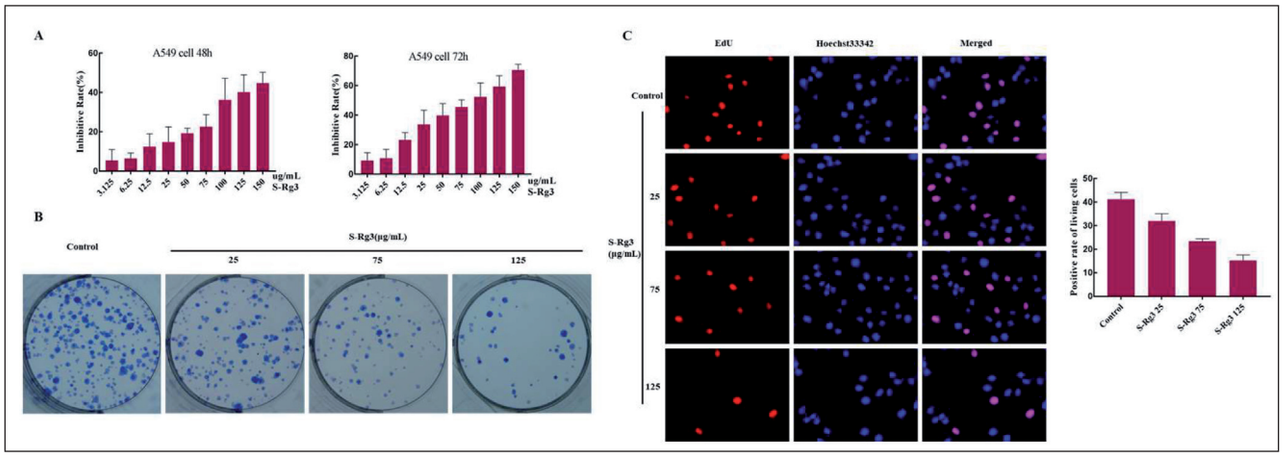

Fig. 1: S-Rg3 inhibits the proliferation of A549 cells. (A) A549 cell viability detected via CCK8 assay after S-Rg3 treatment for 48 and 72 h, respectively. (B) Effect of S-Rg3 on the clonogenic ability of A549 cells. (C) EdU staining to detect the proliferation of A549 cells.

S-Rg3 group than in the control group (15.09% vs. 41.2%, respectively). The results of the CCK8, cell clone formation, and EdU live-cell assays indicate that S-Rg3 has a concentration-dependent inhibitory effect on the proliferation of A549 cells.

2.2. S-Rg3 inhibits the migration and invasion of A549 cells

After the administration of different concentrations of S-Rg3, the ability to migrate of A549 cells was inhibited to different degrees, as observed by wound healing assay (Figure 2A and 2C). Compared with the control group, a low concentration of S-Rg3 interfered with the migration and repair ability of the cells, and the wound healing rate was significantly reduced with increasing concentrations. The inhibition rate was 2.5-fold higher in the 125 μg/mL S-Rg3 group than in the control group (90.9% vs 25.8%, respectively), which suggests that S-Rg3 concentration-dependently inhibits the damage repair ability of cells. Transwell assay (Fig. 2B and 2D) showed that the cell invasion ability was gradually reduced with increasing S-Rg3 concentrations. The inhibition rates were 25.6%, 42.7%, and 65.5% when 25, 75, and 125 μg/mL S-Rg3 were administered, respectively, which indicates that S-Rg3 inhibits the invasion of A549 cells. Thus, wound healing and Transwell assays show that S-Rg3 can concentration-dependently inhibit the migration and invasion of A549 cells.

2.3. S-Rg3 regulates the Hh signaling pathway

The Hh signaling pathway is an important pathway that affects tumor cell proliferation, migration, and invasion. Its key proteins, patched-1 (PTCH1) and GLI1, have marked effects on proliferation and invasion. GLI1 positively regulates the transcription of genes involved in the Hh pathway. Both western blotting (Fig. 3A) and qPCR (Fig. 3B) showed that the expression of GLI1 decreased with increasing S-Rg3 concentrations, whereas that of the negative regulator PTCH1 significantly increased with increasing concentrations. These results suggest that S-Rg3 concentration-dependently inhibits the Hh signaling pathway.

2.4. siRNA-GLI1 interferes with the Hh signaling pathway and enhances the inhibition of EMT by S-Rg3

After the transfection of A549 cells using an siRNA-GLI1 plasmid, wound healing assay (Figure 4A and 4B) showed that, in the

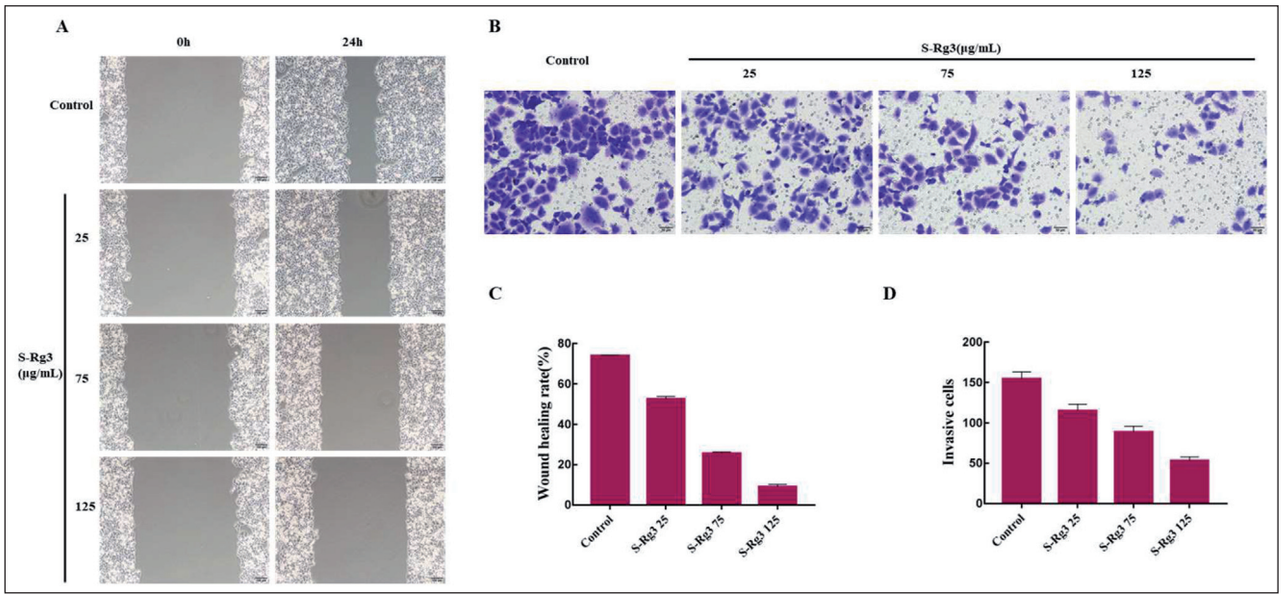

Fig. 2: Inhibitory effect of S-Rg3 on the migration and invasion of A549 cells. (A) Wound healing to detect the effect of S-Rg3 on the migration of A549 cells. (B) Transwell assay to detect cell invasion. (C) Quantitative analysis of the wound healing assay. (D) Quantitative analysis of Transwell assay.

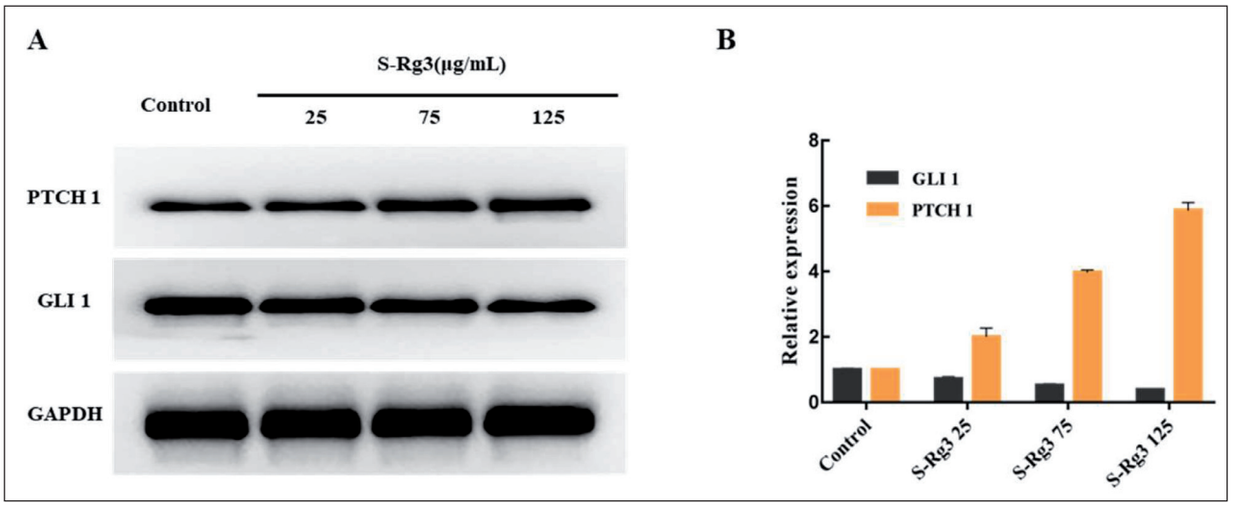

Fig. 3: S-Rg3 inhibited the Hh signaling pathway. A549 cells were treated with S-Rg3, and the expression levels of PTCH1 and GLI1 proteins were detected using western blotting (A) and QPCR (B).

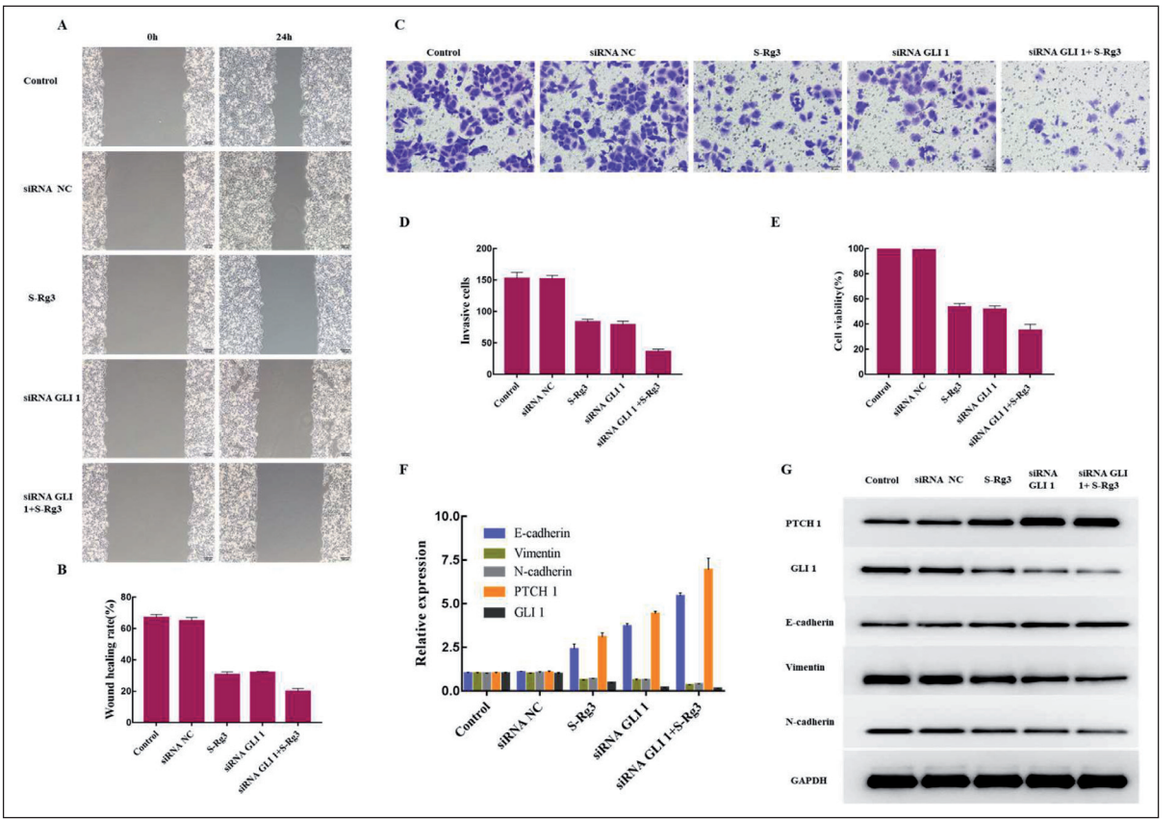

Fig. 4: Inhibition of Hh signaling pathway enhances the effect of S-Rg3 on the proliferation, migration, invasion, and EMT of A549 cells. After silencing the expression of GLI1 with siRNA, (A) the effect of S-Rg3 (75 μg/mL) on the wound of A549 cells and (B) the quantitative expression of wound healing rate were determined. (C) S-Rg3 (75 μg/mL) affects the invasive ability of cells. (D) Quantification of cell invasion ability. (E) S-Rg3 (75 μg/mL) affects the proliferation viability of cells. (F) qPCR to detect the effect of S-Rg3 (75 μg/mL) on the Hh pathway and EMT-related protein levels. (G) Western blotting to analyze whether S-Rg3 (75 μg/mL) regulates the Hh signaling pathway and the expression levels of EMT-related proteins.

siRNA-GLI1 silencing group, wound healing was significantly inhibited in A549 cells compared with that in the blank group, which indicates the successful silencing of GLI1 protein expression. The Transwell (Fig. 4C and 4D) and cell proliferation (Fig. 4E) assays showed similar results. QPCR (Fig. 4F) and western blotting (Fig. 4G) showed that the siRNA-GLI1 group exhibited significantly lower GLI1 levels and higher PTCH1 levels than the control group. Therefore, these results suggest that siRNA-GLI1 silences GLI1 gene expression and, thus, inhibits the Hh signaling pathway. After silencing GLI1 gene expression, the administration of S-Rg3 further inhibited the proliferation of A549 cells (Figure 4E). Wound healing (Fig. 4A and 4B) and Transwell (Fig. 4C and 4D) assays demonstrated that the inhibitory effect of S-Rg3 on the migration and invasion of A549 cells was enhanced by siRNA-GLI1. QPCR (Fig. 4F) and western blotting (Figure 4G) both showed that, after silencing GLI1 gene expression, the administration of S-Rg3 increased the level of E-cadherin and decreased the levels of N-cadherin and vimentin; After the inhibition of the Hh signaling pathway, the inhibitory effect of S-Rg3 on EMT was enhanced. Therefore, the successful inhibition of the Hh signaling pathway by silencing GLI1 gene expression could enhance the inhibition of the proliferation, migration, and invasion of and EMT in A549 cells by S-Rg3.

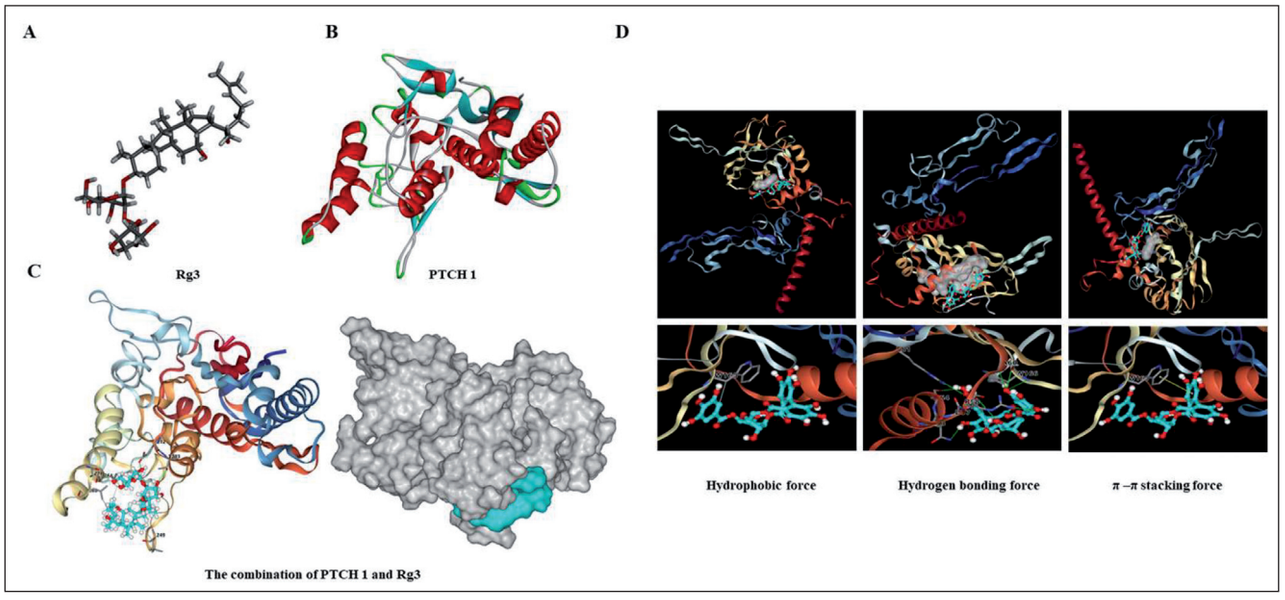

Fig. 5: Molecular docking of Rg3 with PTCH1 protein. (A) Structure diagram of the Rg3 molecule. (B) Pattern diagram of the PTCH1 protein. (C) Binding distribution of PTCH1 protein and Rg3. (D) Binding force between PTCH1 protein and Rg3 molecule.

2.5. Rg3 binds stably to PTCH1 to regulate the Hh signaling pathway

Molecular docking revealed that the Rg3 (Fig. 5A) molecule was stably bound to the PTCH1 protein (Fig. 5B) in a groove on the protein surface (Fig. 5C). The Trp166 of the PTCH1 protein had strong hydrophobic interactions, hydrogen bonding, and π-π stacking forces with Rg3 (Fig. 5D). Additionally, its Ser54, Asp57, Arg81, Arg58, Ala60, and Asn53 bound to Rg3 molecules stably by hydrogen bonding. These results show that Rg3 can bind stably to PTCH1 and affect the Hh signaling pathway *via* the regulation of PTCH1 activity.

3. Discussion

The use of TCM against tumors has become a research hot spot, and research on the underlying mechanisms of action is increasing. Numerous experimental studies have shown that TCM exerts antitumor effects via various mechanisms, including the promotion of apoptosis, inhibition of tumor angiogenesis, inhibition of metastasis, and regulation of the tumor microenvironment. For example, Li et al. showed that the Chinese herbal medicine magnolol blocks the cell cycle, inhibits the growth, and induces the mitochondria-associated apoptosis of gallbladder cancer cells via the upregulation of p53 and p21 levels and downregulation of cyclin D1, CDC25A, and Cdk2 levels (Li et al. 2015; Hong and Mo 2018). Moreover, it was observed that forsythin regulates the proliferation and apoptosis of NSCLC cells through AMPK/ERK/NF-κB (Wu et al. 2020). It has also been demonstrated that bufalin inhibits the EMT and metastasis of human lung adenocarcinoma A549 cells *via* the downregulation of the expression of TGFβ receptors (Zhao et al. 2015).

Shenyi capsule is one of the major adjuvant drugs used in chemotherapy for antitumor treatment, with ginsenoside Rg3 being its main active ingredient. It can not only alleviate the adverse effects caused by chemotherapy and improve the survival quality of patients but also improve the symptoms of *qi* deficiency and enhance the immunity of patients, thereby prolonging their life (Yang and Chen 2020). Moreover, the combination of drugs can boost the antitumor efficiency of treatment.

Additionally, ginsenoside Rg3 has received increased attention in various fields and its mechanism of action has been widely studied. For example, Zhang et al. showed that ginsenoside Rg3 can reduce post-ovariectomy-induced osteoporosis via the AMPK/mTOR signaling pathway (Zhang et al. 2020). Moreover, Rg3 can promote the regression of liver fibrosis by reducing inflammation-mediated autophagy (Liu et al. 2020), and regulate DNA damage in NSCLC via the activation of the VRK1/P53BP1 pathway (Liu et al. 2019), and inhibit EMT in lung cancer *via* the downregulation of FUT4 expression (Tian et al. 2016). However, the effect of Rg3 on the Hh signaling pathway has not been reported.

In our study, the cell proliferation assay (Fig. 1) showed that the inhibition rate increased with the increase in S-Rg3 concentration. After 72 h of treatment with 3.125 μg/mL to 150 μg/mL S-Rg3, the inhibition rate increased 7.7-fold, from 9.19% to 70.64%, respectively. Moreover, S-Rg3 had an outstanding inhibitory effect on the migration and invasion of A549 cells (Fig. 2). The Hh signaling pathway is associated with the proliferation and metastasis of tumor cells; thus, we explored the correlation between S-Rg3 and Hh signaling. Our experimental data confirmed that S-Rg3 regulated the expression of Hh pathway-related proteins; it increased the expression level of PTCH1 and decreased that of GLI 1, thereby inhibiting the Hh signaling pathway (Fig. 3). Therefore, we suggested that S-Rg3 could regulate the Hh signaling pathway to inhibit the proliferation and metastasis of A549 cells. Additionally, siRNA-GLI1 was used to interfere with A549 cells and inhibit the Hh pathway; when administered simultaneously with S-Rg3, it enhanced the inhibition of cell proliferation, migration, invasion, and EMT (Fig. 4). This suggests that, S-Rg3 inhibition of lung cancer cell proliferation, migration, invasion, and EMT by interfering with the Hh signaling pathway. In addition, the observation is not only regulated by Hh pathway, but may also involve other relevant signaling pathways. Notably, siRNA-GLI1 inhibited the Hh signaling pathway and regulated the expression of EMT-related proteins in A549 cells (Figs. 4F and 4G). As reported previously (Ding et al. 2021), EMT acts downstream of Hh signaling; therefore, with the inhibition of the Hh signaling pathway, EMT was also inhibited.

In conclusion, our results reveal that 20(S)-ginsenoside Rg3 inhibits the Hh signaling pathway and, thus, the proliferation, migration, and invasion of and EMT in lung cancer cells; however, this is not the sole signaling pathway that S-Rg3 affects.

4. Experimental

4.1. Cell culture and treatment

Human lung adenocarcinoma cell line A549 was purchased from the Cell Bank of the Chinese Academy of Sciences (Shanghai, China). The cells were cultured in flasks containing Dulbecco's Modified Eagle Medium (DMEM; Gibco, Grand Island, NY, USA) and 10% fetal bovine serum (FBS; Gibco, Grand Island, NY, USA) at 37 °C under 5% CO_2.

4.2. CCK8 cell proliferation assay

A549 cells in the logarithmic growth phase were digested, counted, and prepared as a suspension at a concentration of 5×10^4 cells/mL; inoculated into a 96-well cell culture plate with 100 µL of cell suspension per well; and incubated at 37 °C in a 5% CO_2 incubator for 24 h. The drug was diluted with complete medium to the desired concentration, and 100 µL of the corresponding drug-containing medium was added to each well. A negative control group was also established. The 96-well cell culture plate was incubated at 37 °C in a 5% CO_2 incubator for 48 and 72 h and then stained with CCK8 (CP736, Dojindo Laboratories, Kumamoto, Japan); 10 µL of CCK8 was added to each well, and incubation was continued for 3 h with gentle mixing for 10 min on a shaker. The absorbance value of each well was read with an enzyme-linked immunosorbent assay reader.

4.3. Clone formation

Cells in the logarithmic growth phase were dispersed into a single-cell suspension and counted. The cell suspension was diluted in multiples of gradients and inoculated with 500 cells in a 6-well cell culture plate containing 2 mL of culture medium, and the cells were dispersed evenly. The cell culture plate was transferred into a CO_2 incubator and left to adhere for 24 h at 37 °C, 5% CO_2, and saturated humidity. The groups were treated with drugs for 48 h and then cultured with fresh medium. After 12 days, the culture was discarded, terminated, carefully washed twice with phosphate-buffered saline (PBS), and fixed with 5 mL absolute ethanol for 15 min. After discarding the fixative, Giemsa staining solution (3121TS, Thermo Fisher Scientific, Waltham, MA, USA) was added and the culture was incubated for 10–30 min. The staining solution was slowly rinsed away with running water and the plate was air-dried. The clones were counted directly by observation, and 50 or more cell clusters were considered as a clone.

4.4. Edu staining assay

PBS containing 4% paraformaldehyde (50 µL) was added to a 96-well plate containing A549 cells and incubated for 30 min at room temperature, and the fixative was discarded. Next, 50 µL of 2 mg/mL glycine was added and incubated for 5 min on a decoloring shaker, and the glycine solution was discarded. PBS (100 µL) was added and washed for 5 min on a shaker, after which the PBS was discarded and 200 µL of 1× Apollo® staining solution (KGA337, Jiangsu KeyGEN BioTECH Co., Ltd, Nanjing, China) was added to each well and incubated for 30 min at room temperature in the dark; the staining solution was then discarded. PBS containing 0.5% Triton X-100 (100 µL) was added to rinse the cells 2–3 times on a shaker for 10 min each time, and the penetrant was discarded. Deionized water was used to dilute reagent F at a ratio of 100:1, and an appropriate quantity of 1× Hoechst 33342 solution was prepared and stored in the dark. Next, 100 µL of 1× Hoechst 33342 solution was added to each well and incubated for 30 min on a shaker at room temperature in the dark, the staining solution was discarded, and 100 µL of PBS was added to wash the cells 1–3 times. After washing, 100 µL of PBS was added to each well, and a high-content cell imaging system (magnification 200×) was used for detection.

4.5. Wound healing assay

Cells in the logarithmic growth phase were digested and inoculated into a six-well plate and cultured overnight, and a sterile pipette tip was used to scratch the cell surface. The cells were washed with PBS to remove floating cells. The cells were incubated with a certain concentration of drug diluted with culture medium in a cell incubator. After 48h, the cells were removed and photographed (magnification 200×), and the cell migration distance was measured.

4.6. Transwell assay

Cells in a 24-well plate were removed from the serum and starved for 24 h by incubation in incomplete medium. The incomplete medium was used to double the dilution of Matrigel (356234, BD Biosciences, Franklin Lakes, NJ, USA) that has been melted overnight at 4 °C. Next, 30 µL of diluted Matrigel was added to the upper chamber of the Transwell chambers and incubated at 37 °C for 120 min to polymerize the Matrigel. The cells were digested and counted, and the cell density was adjusted to 1×10^5 cells/mL using incomplete medium. The cell suspension (100 µL) was added to the upper chamber of the Transwell chambers, and 500 µL of medium containing 20% FBS with different formations was added to the lower chamber. The 24-well cell culture plate was incubated in a 5% CO_2 incubator at 37 °C for 48 h. Stromal gel and cells in the upper chamber were wiped off with a cotton swab. The Transwell chamber was removed, inverted, and air-dried; 500 µL of 0.1% crystalline violet was added to the 24-well plate, in which the chambers were placed so that the membrane was submerged in the dye, and removed after incubation for 30 min at 37 °C. After washing the membrane with PBS, photographic images were obtained in three fields of view on the well (magnification 200×), and counted.

4.7. Western blot

After collecting the drug-treated cell samples, proteins were extracted using a total protein extraction kit (KGP250, Jiangsu KeyGEN BioTECH Co., Ltd.), and the protein concentration was determined using the BCA protein content assay kit (KGA902, Jiangsu KeyGEN BioTECH Co., Ltd.). The proteins were separated via SDS-PAGE in 1 × Tris-Gly electrophoresis buffer with approximately 30 µg of total protein per well. Electrophoresis was initially performed at 60 V, which was increased to 90 V when the protein sample entered the separation gel. Proteins in the gel were transferred to a nitrocellulose membrane that had been wetted with methanol and transfer solution. The membrane was washed with Tris-buffered saline containing Tween-20 for 10 min three times, and blocking solution containing 5% skim milk powder was added and shaken for 1.5–2 h on a shaker. After blocking, the membranes were washed with TBST for 10 min three times. The membrane was incubated with primary antibody overnight at 4 °C on a shaker. The next day, the membrane was washed thrice for 10 min with TBST, and the secondary antibody diluted with blocking solution was added. The membrane was shaken for 1–2 h at room temperature and then washed three times with TBST for 5–10 min. Immunoblotting was performed using an ECL chemiluminescence kit (KGP116, Jiangsu KeyGEN BioTECH Co., Ltd.).

4.8. Small interfering RNA (siRNA) transfection

Diluted Lipofectamine 3000 (L3000015, Invitrogen, Carlsbad, CA, USA) and siRNA were gently mixed well, incubated at room temperature for 20 min, and added into a six-well plate containing cells. After mixing these solutions gently, the plate was incubated for 4–6 h. After incubation, the medium containing the plasmid-Lipofectamine 3000 mixture in the wells was removed and replaced with fresh medium; the plate was placed in a 37 °C CO_2 incubator for 48 h.

4.9. Molecular docking

The structure of the PTCH1 protein was retrieved from the Protein Data Bank, and the crystal structure with PDB code 6RTW was used for subsequent molecular docking (Jameson et al. 1999). The initial structure was processed with AutoDock Tools 1.5.6 (Sanner 1999) to preserve the original charge of the protein and generate the pdbqt file for docking.

The structure of the docked ligand ginsenoside RG3 (CAS number 14197-60-5) was obtained from the NCBI database. The molecular structure was optimized for subsequent molecular docking using the MOPAC program (Stewart 1990), and the ligand structure was processed using AutoDock Tools 1.5.6 to generate the pdbqt file for docking.

Molecular docking was performed using the AutoDock 4.2.6 (Morris et al. 2009) package. The center coordinates of the docking box were set to (20.50, 16.23, −24.08), and the number of grid points in each XYZ direction was set to 200 × 200 × 200, so that the docking box enclosed the entire lactoferrin. The number of docking times was set to 500, and the remaining parameters were used as default values. All calculations were completed on the Mol Designer molecular simulation platform.

The resultant molecular docking may have unreasonable atomic contacts in the spatial structure. Energy optimization can be used to release these forces, further stabilizing the structure. Energy optimization was performed using the Amber14 force field in two steps: a 1000-step steepest descent method, followed by a 500-step conjugate gradient method to optimize the structure, and the final result was used as a model for subsequent analysis.

4.10. Statistical analysis

All assays were repeated three times, and the results are expressed as the mean ± standard deviation(SD). The *t*-test was used for statistical analysis, and $p < 0.05$ was considered to indicate statistical significance.

Acknowledgments: This work was supported by Suqian Sci & Tech Program (S201725).

Conflicts of interest: The authors declare that they have no competing interests.

References

Bailey JM, Mohr AM, Hollingsworth MA (2009) Sonic hedgehog paracrine signaling regulates metastasis and lymphangiogenesis in pancreatic cancer. Oncogene 28: 3513–3525.

Belgacem YH, Borodinsky LN (2015) Inversion of sonic hedgehog action on its canonical pathway by electrical activity. Proc Natl Acad Sci USA 112: 4140–4145.

Cao L, Xiao X, Lei J, Duan W, Ma Q, Li W (2016) Curcumin inhibits hypoxia-induced epithelialmesenchymal transition in pancreatic cancer cells via suppression of the hedgehog signaling pathway. Oncology Rep 35: 3728–3734.

Chen X, Lingala S, Khoobyari S, Nolta J, Zern MA, Wu J (2011) Epithelial mesenchymal transition and hedgehog signaling activation are associated with chemoresistance and invasion of hepatoma subpopulations. J Hepatol 55: 838–845.

Dai J, Ai K, Du Y, Chen G (2011) Sonic hedgehog expression correlates with distant metastasis in pancreatic adenocarcinoma. Pancreas 40: 233–236.

Ding J, Li HY, Zhang L, Zhou Y, Wu J (2021) Hedgehog signaling, a critical pathway governing the development and progression of hepatocellular carcinoma. Cells 10: 123.

Ferlay J, Colombet M, Soerjomataram I, Parkin DM, Pieros M, Znaor A, Bray F (2021) Cancer statistics for the year 2020: an overview. Int J Cancer doi: 10.1002/ijc.33588.

Gao XJ, Liu JW, Zhang QG, Zhang JJ, Xu HT, Liu HJ (2015) Nobiletin inhibited hypoxia-induced epithelial-mesenchymal transition of lung cancer cells by inactivating of notch-1 signaling and switching on mir-200b. Pharmazie 70: 256–262.

Hien TT, Kim ND, Kim HS, Kang KW (2010) Ginsenoside rg3 inhibits tumor necrosis factor-alpha-induced expression of cell adhesion molecules in human endothelial cells. Pharmazie 65: 699–701.

Hong ZD, Mo ZX (2018) 11 Kinds of signal pathways in anti-tumor mechanism of Traditional Chinese Medicine. Chin J Exp Trad Med Form 24: 205–218.

Jameson GB, Anderson BF, Norris GE, Thomas DH, Baker EN (1999) Structure of human apolactoferrin at 2.0 a resolution. refinement and analysis of ligand-induced conformational change. Acta Crystallogr D Struct Biol 55: 1108.

Li J, Lu J, Ye Z, Han X, Zheng X, Hou H, Chen W, Li X, Zhao L (2017) 20(s)-rg3 blocked epithelial-mesenchymal transition through dnmt3a/mir-145/fscn1 in ovarian cancer. Oncotarget 8: 53375–53386.

Li J, He Y, Cao Y, Yu Y, Chen X, Gao X, Hu Q (2018) Upregulation of twist is involved in gli1 induced migration and invasion of hepatocarcinoma cells. Biol Chem 399: 911–919.

Li J, Zhang Z, Feng X, Shen Z, Wang Z (2021) Stanniocalcin-2 promotes cell emt and glycolysis via activating itgb2/fak/sox6 signaling pathway in nasopharyngeal carcinoma. Cell Biol Toxicol doi: 10.1007/s10565-021-09600-5.

Li M, Zhang F, Wang X, Wu X, Zhang B, Zhang N, Wu W, Wang Z, Weng H, Liu S, Gao G, Mu J, Shu Y, Bao R, Cao Y, Lu J, Gu J, Zhu J, Liu Y (2015) Magnolol inhibits the growth of gallbladder cancer cells via the p53 pathway. Cancer Sci 106: 1341–1350.

Liu T, Zuo L, Guo D, Chai X, Xu J, Cui Z, Wang Z, Hou C (2019) Ginsenoside rg3 regulates dna damage in non-small cell lung cancer cells by activating vrk1/p53bp1 pathway. Biomed Pharmakother 120: 109483.

Liu X, Mi X, Wang Z, Zhang M, Hou J, Jiang S, Wang Y, Chen C, Li W (2020) Ginsenoside rg3 promotes regression from hepatic fibrosis through reducing inflammation-mediated autophagy signaling pathway. Cell Death Dis 11: 454.

Morris GM, Huey R, Lindstrom W, Sanner MF, Belew RK, Goodsell DS, Olson AJ (2009) AutoDock4 and AutoDockTools4: Automated docking with selective receptor flexibility. J Comput Chem 30: 2785–2791.

Pan JY, Zhou SH (2012) The hedgehog signaling pathway, a new therapeutic target for treatment of ischemic heart disease. Pharmazie 67: 475–481.

Sanner MF (1999) Python: a programming language for software integration and development. J Mol Graphics Model 17: 57-61.

Scales SJ, de Sauvage FJ (2009) Mechanisms of hedgehog pathway activation in cancer and implications for therapy. Trends Pharmacol Sci 30: 303–312.

Stewart JJ (1990) Mopac: a semiempirical molecular orbital program. J Computer-Aided Mol Design 4: 1–105.

Thiery JP, Acloque H, Huang RYJ, Nieto MA (2009) Epithelial-mesenchymal transitions in development and disease. Cell 139: 871–890.

Tian L, Shen D, Li X, Shan X, Wang X, Yan Q, Liu J (2016) Ginsenoside rg3 inhibits epithelial-mesenchymal transition (EMT) and invasion of lung cancer by down-regulating FUT4. Oncotarget 7: 1619–1632.

Wang Y, Han C, Lu L, Magliato S, Wu T (2013) Hedgehog signaling pathway regulates autophagy in human hepatocellular carcinoma cells. Hepatology 58: 995–1010.

Wu S, Zhang Y, Zhang Y, Chen L, Xu X, Dang Y, Ti X (2020) Phillygenin regulates proliferation and apoptosis of non-small cell lung cancer through by ampk/erk/nf-κb axis. Pharmazie 75: 512–515.

Yang YY, Chen LW (2020) Research progress of Shenyi capsule combined with chemotherapy in the treatment of malignant tumors. World Latest Med Inform 20: 77–78.

Zhang F, Li M, Wu X, Hu Y, Cao Y, Wang X, Xiang S, Li H, Jiang L, Tan Z, Lu W, Weng H, Shu Y, Gong W, Wang X, Zhang Y, Shi W, Dong P, Gu J, Liu Y (2015) 20(s)-ginsenoside rg3 promotes senescence and apoptosis in gallbladder cancer cells via the p53 pathway. Drug Design Devel Ther 13: 3969–3987.

Zhang X, Huang F, Chen X, Wu X, Zhu J (2020) Ginsenoside Rg3 attenuates ovariectomy-induced osteoporosis via AMPK/mTOR signaling pathway. Drug Devel Res 81: 875–884.

Zhao L, Liu S, Che X, Hou K, Ma Y, Li C, Wen T, Fan Y, Hu X, Liu Y, Qu X (2015) Bufalin inhibits tgf-β-induced epithelial-to-mesenchymal transition and migration in human lung cancer a549 cells by downregulating tgf-β receptors. Int J Mol Med 36: 645–652.